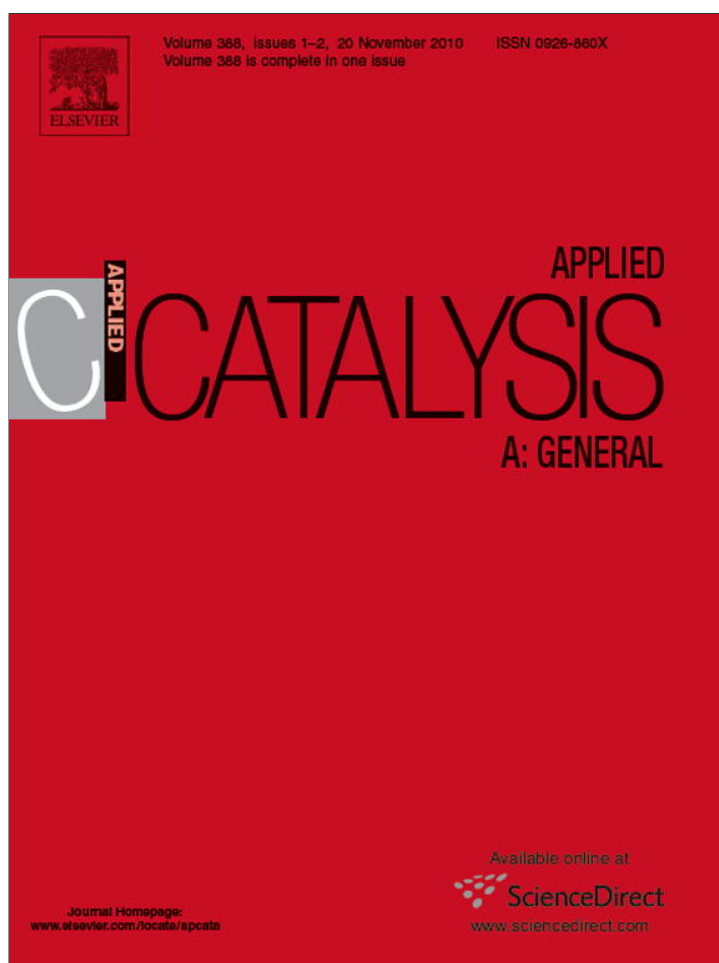


Provided for non-commercial research and education use.
Not for reproduction, distribution or commercial use.

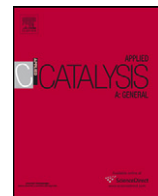


This article appeared in a journal published by Elsevier. The attached copy is furnished to the author for internal non-commercial research and education use, including for instruction at the authors institution and sharing with colleagues.

Other uses, including reproduction and distribution, or selling or licensing copies, or posting to personal, institutional or third party websites are prohibited.

In most cases authors are permitted to post their version of the article (e.g. in Word or Tex form) to their personal website or institutional repository. Authors requiring further information regarding Elsevier's archiving and manuscript policies are encouraged to visit:

<http://www.elsevier.com/copyright>



Catalytic partial oxidation of ethanol on alumina-supported rhodium catalysts: An experimental study

N. Hebben^a, C. Diehm^a, O. Deutschmann^{a,b,*}

^a Institute for Chemical Technology and Polymer Chemistry, Karlsruhe Institute of Technology (KIT), Kaiserstraße 12, D-76128 Karlsruhe, Germany

^b Institute for Nuclear and Energy Technology, Karlsruhe Institute of Technology (KIT), Hermann-von-Helmholtz Platz 1, D-76344 Eggenstein-Leopoldshafen, Germany

ARTICLE INFO

Article history:

Received 21 April 2010

Received in revised form 2 August 2010

Accepted 26 August 2010

Keywords:

Catalytic partial oxidation

Ethanol

Rhodium

Hydrogen production

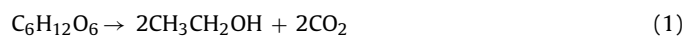
ABSTRACT

The catalytic partial oxidation of ethanol is experimentally studied over an alumina rhodium coated monolithic honeycomb catalyst at short contact times. The product distribution is analyzed as function of carbon-to-oxygen ratio (C/O) for two different space velocities by a variety of simultaneously applied methods such as Fourier transform infrared spectroscopy, sector mass spectrometry, paramagnetic gas analyzer and gas chromatography combined with mass spectrometry. Low C/O resulted in highly selective synthesis gas production, whereas by-products like methane, ethylene, acetaldehyde and diethyl ether became eminent with increasing C/O.

© 2010 Elsevier B.V. All rights reserved.

1. Introduction

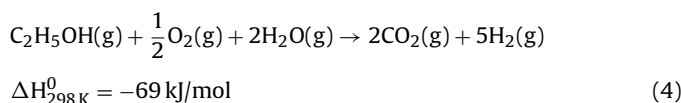
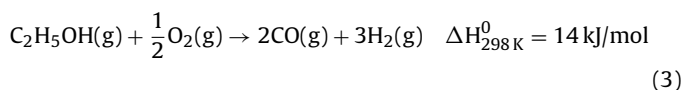
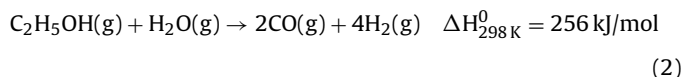
There is a further increasing interest in the reduction of greenhouse gases (as carbon dioxide, methane and nitrous oxide), global warming, as well as in secured energy allocation. One promising of many candidates for the next generation of energy carriers is ethanol; it can be easily obtained in large amounts by fermentation of biomass (Eq. (1)). Furthermore, ethanol has a high energy density and a low toxicity. Moreover, its transport, storage, and distribution are relatively unproblematic.



By converting ethanol into hydrogen-rich gas, it can be used as a hydrogen source for various fuel cells (like polymer electrolyte membrane (PEMFC), solid oxide (SOFC) and molten carbonate fuel cell (MCFC)).

Several studies on hydrogen production by steam reforming (SR, Eq. (2)) [1–8], partial oxidation (POX, Eq. (3)) [9–13], and autothermal reforming (ATR, Eq. (4)) [14–19], also known as oxidative steam reforming (OSR) of ethanol on rhodium coated catalysts have been

published.

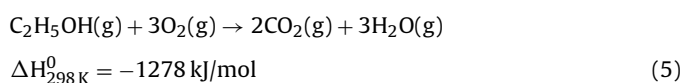


In general, steam reforming of ethanol is a very efficient process to obtain high hydrogen yields. However, a major disadvantage of this method is the fact that steam reforming is a highly endothermic reaction. Consequently, thermal energy must be added to the process in order to achieve high conversion at temperatures around 1100 K. Furthermore, large amounts of steam are required, so higher energy consumption for vaporization of water has to be taken into account. Partial oxidation processes, on the other hand, have fast start up and response times. Moreover, the POX reactor set-up is more compact than the one for steam reforming, because it does not need the additional supply of heat through a heat exchanger. Autothermal reforming combines SR and POX in one reactor and supersedes an external heat supply.

* Corresponding author at: Karlsruhe Institute of Technology (KIT), Institute for Chemical Technology and Polymer Chemistry (ITCP), Engesserstr. 20, 76131 Karlsruhe, BW, Germany. Tel.: +49 721 608 3064; fax: +49 721 608 4805.

E-mail address: deutschmann@kit.edu (O. Deutschmann).

In contrast to POX of aliphatic hydrocarbons such as methane (natural gas), iso-octane (gasoline), and hexadecane (diesel), the partial oxidation of ethanol is slightly endothermic ($\Delta H_{298\text{K}}^0 = +14 \text{ kJ/mol}$). Therefore, only a small amount of fuel can be used for total oxidation (Eq. (5)) to provide heat for autothermal operation.



Even though ethanol represents a renewable energy source, a gentle utilization of resources is appropriate due to economic and ecologic reasons. Thus, if a better understanding of the mechanism of catalytic partial oxidation (CPOX) is achieved an optimized reactor can be developed to enhance the reaction processes. Furthermore, the catalyst formulation itself can be optimized, leading to reduced noble metal loadings and thereby to reduced costs. A prerequisite for the elucidation of reaction mechanisms is the availability of experimental results, obtained in reactors operated at well-defined boundary conditions to allow adequate numerical simulation of the chemical processes as well as heat and mass transfer in the reactor used.

Here, we present the results of an experimental study of CPOX of ethanol on alumina-supported rhodium coated monolithic honeycomb catalysts at short contact times under well-defined experimental conditions. The reactor is designed in such a way, that geometry and operation conditions correspond as good as possible to the assumptions usually to be made in the numerical model. The analytic setup ensures that all supposable species are detected and quantified by gas chromatography combined with mass spectrometry, fourier transform infrared spectroscopy, sector mass spectrometry, and paramagnetic gas analyzer. A special focus of this study is on the formation of by-products, like acetaldehyde and diethyl ether as function of C/O in the range of 0.67 and 1.33. The CPOX reactor is operated autothermally.

2. Experiment

2.1. Experimental setup

The setup is designed to ensure reproducible experimental investigations of catalytic partial oxidation of different fuels by establishing well-defined initial and boundary conditions. It allows the evaporation and thorough mixing of the fuel with synthetic air; a homogeneous, pulse-free mixture is fed into the catalyst at a radially uniform temperature profile. The feed temperature of the fuel-mixture is kept below the auto-ignition temperature to avoid gas-phase reactions upstream the catalyst. The flow reactor consists of a 50 cm long quartz tube with an external diameter of 21.5 mm and is placed inside a furnace (35 cm in length). A detailed specification of the reactor configuration is published elsewhere [20,21].

2.2. Catalyst

For the experimental investigations, a commercially manufactured monolithic honeycomb catalyst is used. It is 10 mm in length and 19 mm in diameter with a cell density of 900 channels per square inch (cpsi) and is positioned 21 cm downstream the mixture inlet. An uncoated alumina foam monolith with 85 pores per linear inch (ppi) is placed in front of the catalyst as flow homogenizer. An uncoated honeycomb monolith (600 cpsi) is also placed behind the catalyst. Both uncoated monoliths also serve as heat shields to reduce radiation heat losses as well as holders for the thermocouples (front face: Type K, back face: Type N) and are 10 mm in length and 19 mm in diameter. A ceramic cloth (approx. 1 mm thick) is

wound around the catalyst and the two uncoated monoliths to prevent gas bypass.

The catalyst is characterized by measuring the BET surface area with nitrogen adsorption at 77 K (BELSORP-miniII, BEL JAPAN, Inc.) and scanning electron microscope (SEM) analysis (HITACHI S-3400N electron microscope). The catalytic active surface area is investigated by CO-chemisorption (1 CO bonded to 1 Rh, in-house manufactured experimental set-up), as well as H₂-chemisorption (1 H₂ bonded to 2 Rh, sorption meter Z10/97-Autosorb-1-C, Quantachrome), and flame atomic absorption spectroscopy (AAS, HITACHI Z-6100).

2.3. Analytical setup

The product stream is analyzed by a variety of simultaneously applied methods like process Fourier transform infrared spectroscopy (FT-IR, MKS MultiGas 2030), sector mass spectrometry (V&F, H-Sense), paramagnetic gas analyzer (ABB, Magnos 206) and gas chromatography combined with mass spectrometry (GC/MS, Agilent 6890N Network Gas Chromatograph combined with a Agilent 5973 Mass Selective Detector). The advantage of the presented GC/MS measurement system is the possibility to detect the complete product distribution, as well as the unconverted fuel, while the other analytical tools can also be used for transient measurements [20]. The total product stream of ethanol CPOX contains a large variety of different species like water, hydrogen, nitrogen, carbon monoxide and dioxide, as well as hydrocarbons and oxygenated hydrocarbons. The GC/MS allows simultaneous detection of nearly all chemical species in the product gas mixture with a total analysis time of 20 min. The system used here is equipped with a three-column-switching system in combination with three detectors (thermal conductivity detector (TCD), flame-ionization detector (FID) and mass selective detector (MS)). High purity helium ($\geq 99.999\%$), additionally cleaned with a superior helium gas purifier, serves as carrier gas. A schematic diagram of the GC/MS measurement system is shown in Fig. 1.

The product gas sample enters the GC/MS system with a temperature of 473 K and is regulated by controlled heating pipelines. The sample loop and the split/splitless-injector are heated up to 473 K to prevent that any species of the sample precipitates. After passing the sample loop and the split/splitless-injector the sample flows into the oven with the columns. As soon as the smaller chemical species (hydrogen, nitrogen, oxygen, carbon monoxide, carbon dioxide, water, methane, C₂- and C₃-isomers) pass the first column, DB-5MS (Agilent J&W GC Column (30 m × 0.329 mm × 0.25 μm)), the Deansswitch-valve is closed and the bigger species, like higher hydrocarbons (C_xH_y, 4 ≤ x ≤ 16) and oxygenated hydrocarbons (as ethanol, acetaldehyde, acetone, diethyl ether) are detected in parallel with the FID and MS.

The smaller species are detected with the TCD. For this purpose the sample runs through the second column, HP-Plot Q (Agilent J&W GC Column (30 m × 0.323 mm × 20.00 μm)). As soon as hydrogen is detected, the 6-port-valve is used and N₂, O₂, CO, CH₄ are stored temporarily at the third column, HP-MoleSieve 5A (Agilent J&W GC Column (30 m × 0.320 mm × 25.00 μm)), and CO₂, H₂O, C₂- and C₃-isomers are measured. Finally the species from the third column are analyzed.

To facilitate the separation of the product stream through the columns a seven step temperature ramp (start: 308 K, end: 523 K) is applied.

2.4. Experimental procedures and conditions

The molar carbon-to-oxygen ratio (C/O) serves as parameter to describe the feed composition, which is defined as the quantity of C atoms entering the reactor with ethanol divided by the number

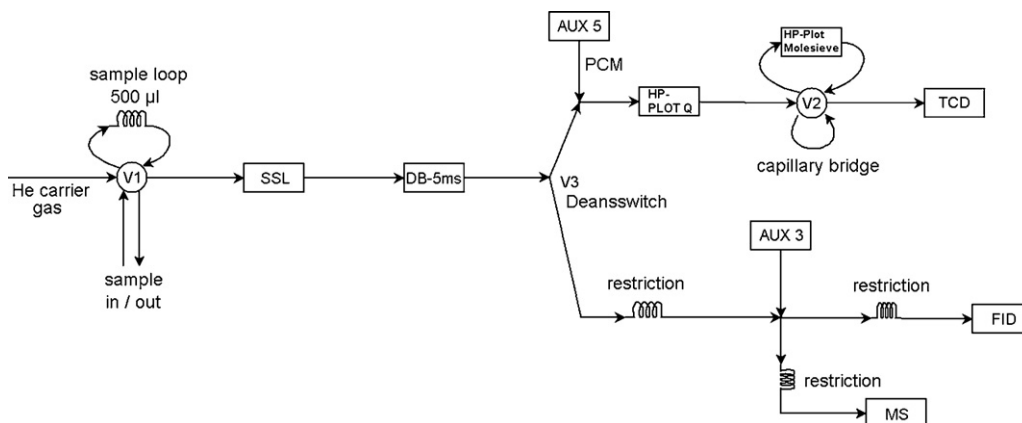


Fig. 1. Scheme of the GS-MS measurement system.

of O atoms entering with oxygen and ethanol. In this context a C/O of 1.00 represents partial oxidation (Eq. (3)). For this study, C/O is varied between 0.67 ($C_2H_5OH + O_2$) and 1.33 ($2C_2H_5OH + (1/2)O_2$), while the total flow rate is kept constant. Two different total flow rates are investigated, 2 and 4 standard liters per minute (SLPM), which correspond to a gas hourly space velocity (GHSV) of 42,325 and 84,650 h^{-1} , respectively. The contact time of the fuel compositions at the catalyst is 11 ms for a flow rate of 4 SLPM and 21 ms for 2 SLPM. The reactants are diluted with 80 vol.% nitrogen. Fuel and synthetic air are fed to the reactor by the use of controlled heating pipelines, regulated to an entering temperature of 463 K. The reactor is operated in a furnace at atmospheric pressure and preheated to 523 K. As soon as light-off occurs, the furnace is turned off and the reactor is operated autothermally.

The product distribution is monitored by FT-IR, H-Sense, gas analyzer and the temperature by thermocouples (at front and back face of the catalyst) as function of time. When the steady state has been reached, the product composition is analyzed by GC/MS. After the measurement, the catalyst is regenerated through temperature programmed oxidation. Without regeneration the catalyst would slowly be covered by a carbonaceous overlayer (coking) at large C/O. Regeneration also ensures equal starting conditions for all C/O and flow rates.

The ethanol conversion $X_{ethanol}$ and selectivity of products S_{x_i} are defined by:

$$X_{ethanol} = \frac{(n_{ethanol})_{in} - (n_{ethanol})_{out}}{(n_{ethanol})_{in}} \quad (6)$$

with $(n_{ethanol})_{in}$ = moles of ethanol in the feed and $(n_{ethanol})_{out}$ = moles of ethanol in the outlet stream,

$$S_{x_i} = \frac{a_i(n_{x_i})_{produced}}{\sum_i a_i(n_{x_i})_{produced}} \quad (7)$$

where $(n_{x_i})_{produced}$ = moles of produced species x_i (x_i : H_2 , CO , CO_2 , H_2O , CH_4 etc.) and a_i number of H and C atoms of the molecule x_i for H- and C-selectivity, respectively.

At 4 SLPM, each C/O is investigated using three identical catalyst samples (different charge of the same catalyst system), at 2 SLPM using at least two. All C/O are analyzed twice on each catalyst sample. The experiments have a high reproducibility and the results presented here are the average measurement values. The mean error of the average values of the main product's concentrations is below 4.0% for low C/O. For large C/O the error is less than 7.5%. The element balance for C, H, and O is closed.

In order to check for any gas-phase reactions in front of the catalyst, experiments with blank (not coated with catalyst) monoliths

are carried out for a C/O of 1.00 with an inlet temperature of 498 K. No decomposition of fuel is observed.

3. Results

3.1. Catalyst characterization

The honeycomb monolith is made out of cordierite and the inner walls of the channels are coated with rhodium as the catalytic active component dispersed in a γ -alumina washcoat. Scanning electron microscope analysis show that most of the washcoat is deposited in the corners of the rectangular shaped channel where the washcoat is up to 150 μm thick. The thickness of the washcoat in the remaining parts of the channel wall area is around 20 μm .

The average BET surface area of the used catalyst is 45.7 m^2/g . The CO-chemisorption measurements lead to a rhodium metal dispersion of 49%. For H_2 -chemisorption experiments, the measured average value for the metal dispersion is 53% and leads to a catalytic active surface area of 0.56 m^2/g . The AAS measurements lead to an average catalyst weight loading of Rh of 0.24 wt.%.

3.2. Reactor conditions

The CPOX reactor is operated autothermally. Fig. 2 shows the measured catalyst inlet and outlet temperature as well as the calculated adiabatic reaction temperature. For a total flow rate of 4 SLPM, the aberration of measured and calculated outlet temperature is between 4 and 36 K depending on the appointed C/O. The differ-

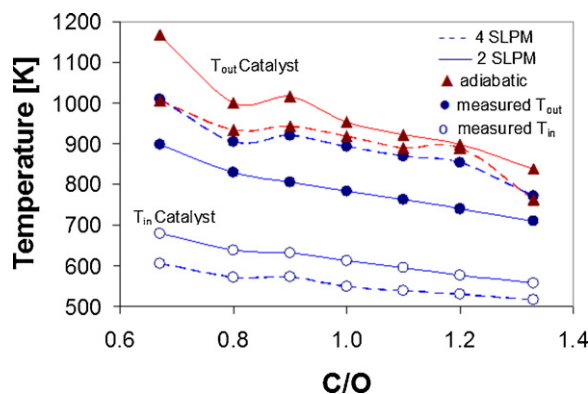


Fig. 2. Measured gas temperature at the catalyst inlet and outlet, as well as the calculated adiabatic outlet temperature as function of C/O for the CPOX of ethanol on alumina-supported Rh based catalysts.

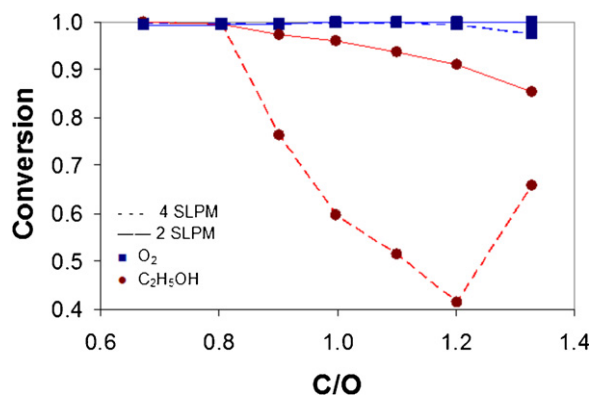


Fig. 3. Experimentally measured fuel conversion as function of C/O for the CPOX of ethanol on alumina-supported Rh based catalysts.

ence between measured and calculated temperature for a flow rate of 2 SLPM lies within the range of 125 and 270 K.

3.3. Product composition

Fig. 3 shows the fuel and oxygen conversion as function of C/O. The oxygen conversion for both flow rates (2 and 4 SLPM) is above 99%, except for C/O of 1.33 (4 SLPM) being 97%. The ethanol conversion decreases with increasing C/O. At a flow rate of 2 SLPM the ethanol conversion is 100% for C/O of 0.67 and drops down to 85% for C/O of 1.33. In the experiments conducted at a flow rate of 4 SLPM, the ethanol conversion decreases from 100% for C/O of 0.67 to 42% for C/O of 1.20 and increases again to 66% for C/O of 1.33.

Figs. 4 and 5 present the experimental H- and C-selectivities for the main products H₂, H₂O, CO, and CO₂ as function of C/O for the two total flow rates of 4 and 2 SLPM (Fig. 4 shows 4 SLPM and Fig. 5 shows 2 SLPM). Figs. 6 and 7 show the experimental selectivity for the side products CH₄, C₂H₄, CH₃CHO, and (C₂H₅)₂O as function of C/O, also for 2 and 4 SLPM. The selectivities of the by-products C₂H₆, and C₃H₆ occur in traces only and are not pictured. C₃H₇CHO (not shown) occurs in traces up to a C/O of 1.00 and increases slightly with the C/O, depending on the (C₂H₅)₂O production.

The H₂O selectivity rises with increasing C/O for both flow rates. CH₄ selectivity is very low and nearly of the same magnitude for 2 and 4 SLPM. It has a maximum for C/O of 1.00 at around 10%.

The by-products C₂H₄, CH₃CHO, and (C₂H₅)₂O increase with C/O. The C₂H₄ selectivity is higher for the flow rate of 2 SLPM than for 4 SLPM. On the other hand the selectivity for (C₂H₅)₂O is higher for 4 SLPM than for 2 SLPM. At 2 SLPM, the production of C₃H₇CHO is higher than for 4 SLPM.

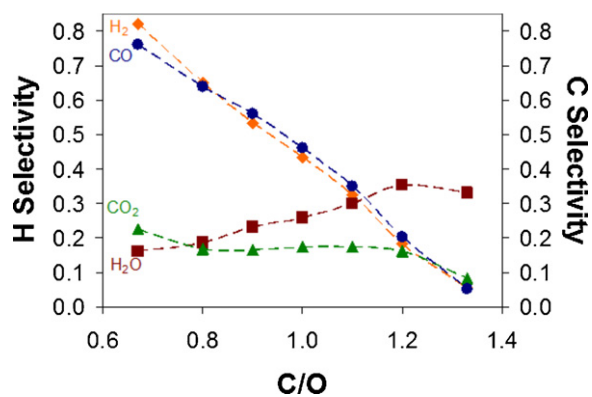


Fig. 4. Experimental H- and C-selectivities of the main products as function of C/O for the CPOX of ethanol on alumina-supported Rh based catalysts for 4 SLPM.

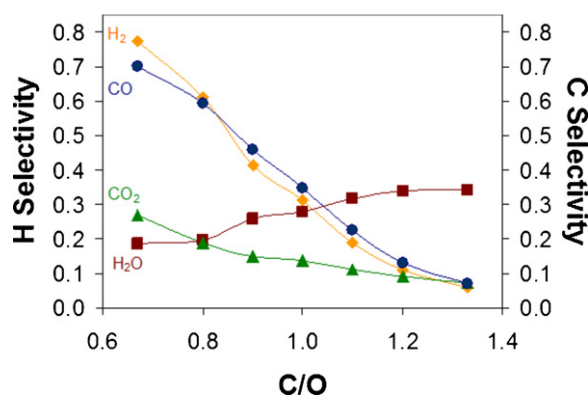


Fig. 5. Experimental H- and C-selectivities of the main products as function of C/O for the CPOX of ethanol on alumina-supported Rh based catalysts for 2 SLPM.

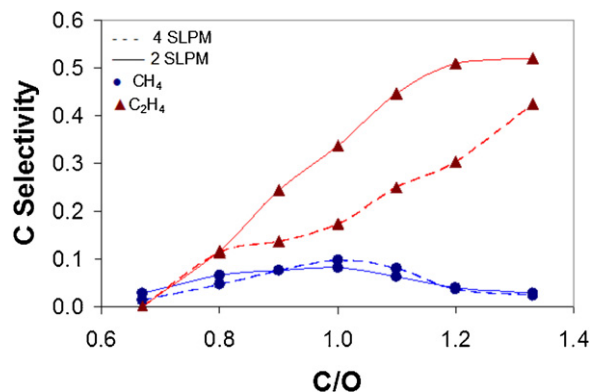


Fig. 6. Experimental C-selectivity of the hydrocarbon side products as function of C/O for the CPOX of ethanol on alumina-supported Rh based catalysts for 2 and 4 SLPM.

4. Discussion

4.1. Thermodynamic equilibrium

The results of the thermodynamic equilibrium calculations are presented in Figs. 8–10; all computations are carried out with DETCHEM^{EQUIL} [22]. The species spectrum used in the calculations is nitrogen, hydrogen, oxygen, water, carbon monoxide, carbon dioxide, methane, acetylene, ethylene, ethane, propylene, formaldehyde, acetaldehyde, butanal, methanol, ethanol, diethyl ether, acetone, and tetrahydrofuran.

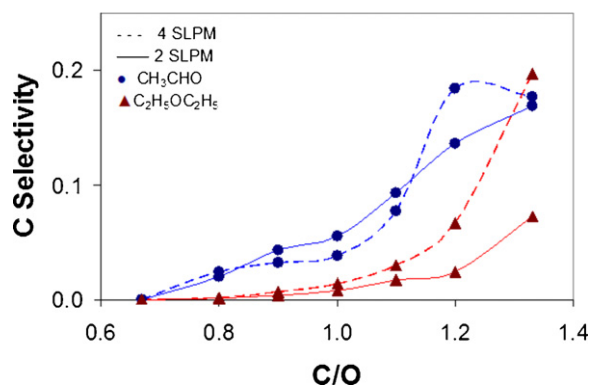


Fig. 7. Experimental C-selectivity of the oxygenated hydrocarbon side products as function of C/O for the CPOX of ethanol on alumina-supported Rh based catalysts for 2 and 4 SLPM.

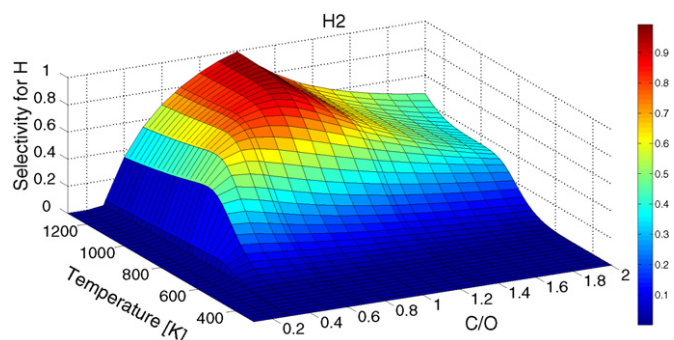


Fig. 8. Computed H-selectivity for H₂ as function of temperature and C/O for ethanol–oxygen mixture at thermodynamic equilibrium.

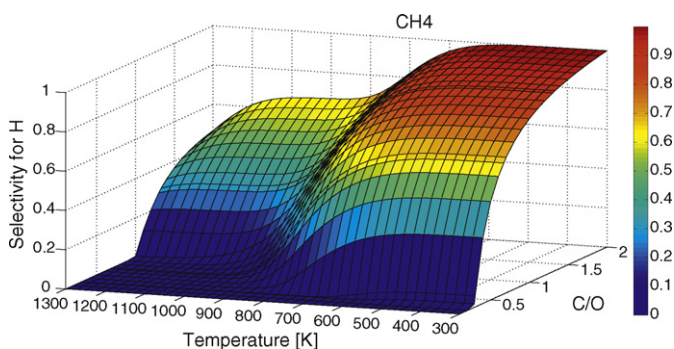


Fig. 9. Computed H-selectivity for CH₄ as function of temperature and C/O for ethanol–oxygen mixture at thermodynamic equilibrium.

The equilibrium products for various C/O and temperatures include H₂, H₂O, CO, CO₂, and CH₄; no other by-products are determined in noteworthy amounts. Oxygen and ethanol are completely converted at thermodynamic equilibrium.

For a C/O of 0.10 the equilibrium species are H₂O and CO₂ only. With increasing C/O the amount of H₂O and CO₂ decreases, while the production of CO, CH₄, and H₂ increases. At a C/O of 1.00, CO and H₂ selectivities have their maxima; for larger C/O H₂ and CO selectivities decrease again and more and more CH₄ is produced. At a C/O of 2.00 and low temperatures, CH₄, CO, and CO₂ are predicted as equilibrium species only. For higher temperatures H₂ and much less amounts of H₂O also are produced.

In comparison with the experimental results, as discussed below, equilibrium is approached for the experimental conditions of C/O of 0.67 only, for both 2 and 4 SLPM. With increasing C/O, the difference between experimental product composition and equilibrium composition increases due to the generation of by-products.

The formation of H₂O deviates from thermodynamic equilibrium with increasing C/O. Experimental CH₄ production is less than

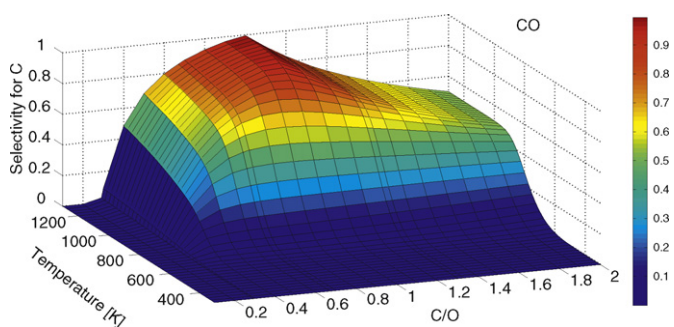
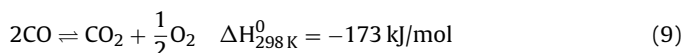
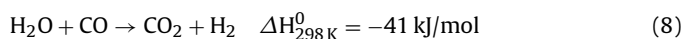


Fig. 10. Computed C-selectivity for CO as function of temperature and C/O for ethanol–oxygen mixture at thermodynamic equilibrium.

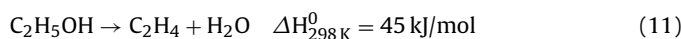
the amount given at equilibrium. Especially for higher C/O, high amounts of CH₄ would be expected from a thermodynamic point of view, but are not observed.

4.2. Product distribution

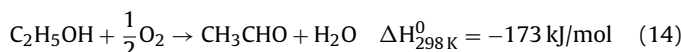
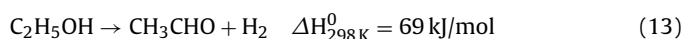
At low C/O, the product distribution is close to equilibrium and the decomposition or oxidation of ethanol investigated on the catalyst involves a mixture of reactions, like partial oxidation (Eq. (3)), total oxidation (Eq. (5)), water–gas shift reaction (Eq. (8)), Boudouard equilibrium (Eq. (9)), steam reforming (Eq. (2)) and dry reforming (Eq. (10)).



At higher C/O, the production of the by-products becomes significant. The ethanol oxidation resulted in dehydration products, namely ethylene (Eq. (11)) and diethyl ether (Eq. (12)), through reactions,



as well as in acetaldehyde formation through dehydrogenation (Eq. (13)) and dehydration (Eq. (14)) reactions.



Ethanol oxidation over $\gamma\text{-Al}_2\text{O}_3$ catalyst leads to dehydrogenation products, especially ethylene and diethyl ether. Aluminium oxide contains several catalytic active centers. On the one hand, there are Brønsted acid sites (hydroxyl groups) and oxygen ions, which may be regarded as the active centers for the unimolecular olefin formation. On the other hand, there are Lewis acid sites (Al³⁺), that, in combination with the hydroxyl groups and the oxygen ions, catalyse the formation of ether through a bimolecular reaction [24]. Consequently, the formation of significant amounts of ethylene and diethyl ether over the investigated catalysts with low Rh-loading, particularly for high C/O, are assigned to the alumina support. This effect also explains the apparently unexpected observation of monotonously rising selectivity of water for increasing C/O. The methane concentration is low for the entire C/O range investigated. At low C/O, methane concentration rises slightly with increasing C/O, however, after passing the maximum at C/O of 1.00, CH₄ concentration decreases again due to the production of the dehydration products.

For 2 SLPM, more ethylene and less diethyl ether are produced compared to the experiments operated at 4 SLPM, which is attributed to interaction of several different effects like higher contact times, temperature, and kinetics, but cannot be separated into single effects at the current state of knowledge.

Production of butanal (not shown) occurs simultaneous with diethyl ether (less than ether); for the experiments at 2 SLPM more butanal is produced than for a flow rate of 4 SLPM. It is explained that diethyl ether is partially converted to butanal on the Rh surface [23].

Fuel conversion continuously decreases with increasing C/O at fuel rich conditions (C/O \geq 1.00); for 2 SLPM higher conversion is observed than for 4 SLPM due to longer residence time. At 4 SLPM, ethanol conversion shows a minimum at C/O of 1.20. For higher C/O the conversion rises again, as a result of increasing dehydration side products yield, such as diethyl ether and ethylene. Also, the

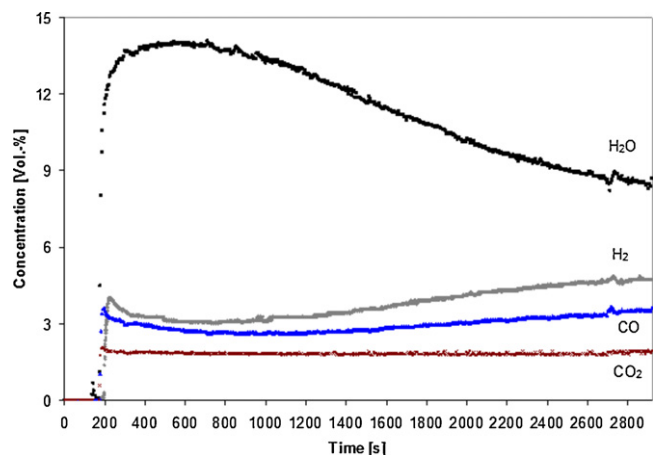


Fig. 11. Concentration profile determined by FT-IR and sector mass spectrometry of the main products as a function of time for C/O of 1.20, start of the experiment at ~ 200 s.

ethanol conversion is influenced by deactivation of the catalyst. Experiments without regeneration of the catalyst (Burn-off of coke) after each experimental run, i. e. for one given flow rate and C/O, lead to lower fuel conversion and consequently different product spectra at C/O above 1.00. Between C/O of 1.00 and 1.20, the time the reactor needs to reach steady state increases (Fig. 11). For C/O of 1.33 the behaviour changes again and the steady state is reached quickly (Fig. 12), as observed for C/O < 1.00.

Another observation of the here presented experiments indicate that the formation of ethylene, diethyl ether and acetaldehyde are surface reactions. Their concentration profiles for high C/O (except for C/O of 1.33) during the time to reach steady state show a decrease. Also, water shows a decrease during that time (Fig. 11). The observed temperatures keep constant after a few minutes and do not change significant during the rest of the experiment run time. At least the decrease of the ethanol conversion and the side product concentrations seemed to be effects of the deactivation of the catalytic active centres of the catalyst. If the formation of the side products would be gas-phase dominated, the deactivation of the catalyst would not have that significant influence. A temperature change would have definitive an influence on the gas-phase reactions, but the temperature during the experiments stayed constant. Also, the results of the gas-phase modelling indicate that the gas-phase reactions play an underpart (see Section 4.4).

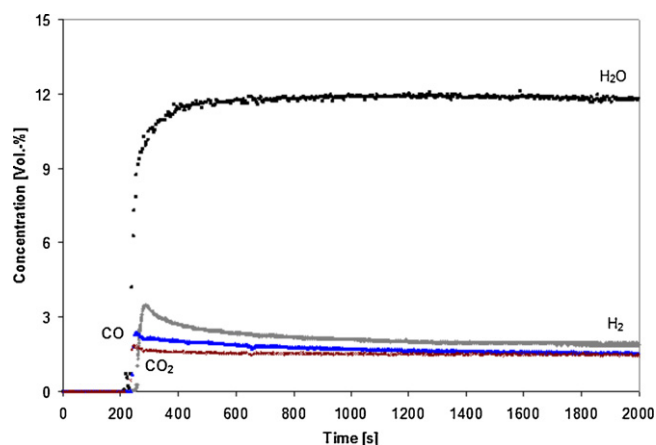


Fig. 12. Concentration profile determined by FT-IR and sector mass spectrometry of the main products as a function of time for C/O of 1.33, start of the experiment at ~ 200 s.

4.3. Catalyst temperature

The observed catalyst temperature depends on several parameters such as flow rate, C/O, heat transfer, and chemical heat release. In general, the temperatures decrease with increasing C/O due to the reduced oxygen amount in the feed, which results in less exothermal total oxidation, which usually appears at the inlet of the catalyst in catalytic partial of hydrocarbon [25,26]. At C/O below 1.00 the oxygen concentration inside the feed is higher than needed for partial oxidation. Thus, total oxidation occurs and provides heat for autothermal operation. For C/O > 1.00 the available oxygen favours partial oxidation, although from a thermodynamic point of view, total oxidation is favoured at lower temperature. In addition, the catalyst back face temperature for the experiments of 2 SLPM is lower than for 4 SLPM; contrariwise the opposite is observed for the catalyst front face temperature. The higher flow velocity cools down the catalyst inlet and shifts the hot reaction zone to the catalyst outlet, so a lower inlet temperature will be observed for 4 SLPM experiments. Furthermore, more heat is produced in the reactor for higher mass flow rates, and the heat loss due to heat conduction and thermal radiation has a stronger impact for lower flow rates. The measured catalyst back face temperature compared to the calculated adiabatic reactor temperature shows that the reactor is operated nearly adiabatically at 4 SLPM but not at 2 SLPM (Fig. 2). The adiabatic reaction temperature calculations are carried out with DETCHEM^{ADIABAT} [22]. The experimentally determined inlet and outlet composition of all detected species (hydrogen, oxygen, water, carbon monoxide, carbon dioxide, methane, ethylene, ethane, acetaldehyde, ethanol, acetone, butanal, and diethyl ether) served as input for the calculations.

4.4. Homogeneous gas-phase reactions

Marinov proposed an elementary gas-phase reaction mechanism to describe high-temperature ethanol oxidation [28]. His model includes 57 species and 370 elementary reaction steps. Christensen et al. [29] investigated noncatalytic POX of ethanol in the range from 873 to 1073 K and compared their experimental results with the Marinov model. They found that the model predicts trends, but does not reproduce their experimental data accurately. Salge et al. [10] also used the model to compare it with blank tube experiments for a C/O ratio of 1.00 at 1173 K. Ethanol was mixed with oxygen and nitrogen at air stoichiometry, without dilution. Comparison of their experimental results with the model shows that the model predicts H₂, H₂O, CO₂, CO, and CH₄ selectivities to within 2%, but the model overpredicts C₂H₄ selectivity and underpredicts CH₃CHO selectivity by 5%. Complete conversion of the fuel at their conditions is predicted.

In the present work, the Marinov model is used in a two-dimensional simulation of a single monolith channel based on the code DETCHEM^{CHANNEL} to study the gas-phase chemistry for high temperatures and to combine these results with the blank experiments done for inlet and oven temperature [22]. This code simulates the steady state reactive flow through a cylindrical channel using the boundary layer approximation [30,31]. The measured temperature of the oven and at the catalyst inlet and outlet are used to roughly estimate the temperature profile in the reactor, which is applied in the simulation of the reactive gas-phase flow through the reactor. The estimated profile is given in Fig. 13. At these conditions, very little conversion of ethanol (<0.4%) and oxygen (<0.3%) are predicted by the model in both cases (2 and 4 SLPM), except in the case of 4 SLPM for a C/O of 0.67, where an ethanol conversion of 19.1% and an oxygen conversion of 9.8% is predicted, see Fig. 13. In this case, the products are formaldehyde, acetaldehyde, methane, ethane, water, and hydrogen peroxide, which are produced in the hot zone of the catalyst.

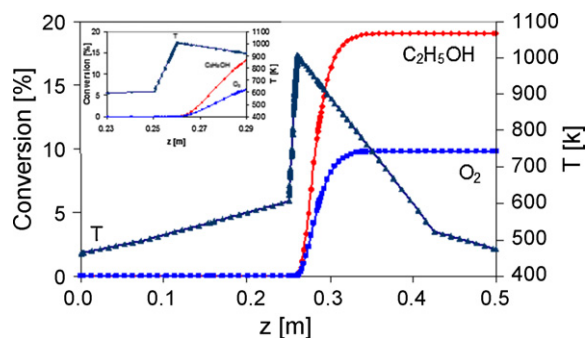


Fig. 13. Numerically predicted conversion of ethanol and oxygen in the gas-phase (without a catalyst) as a function of the reactor length for C/O of 0.67 at 4 SLPM and the experimentally determined temperature profile. Catalyst position: 0.25–0.26 cm.

Also ‘worst case’ isothermal simulations with the measured outlet temperature are performed for the catalyst length of 0.01 m. For the flow rate of 2 SLPM basically no conversion of ethanol (<0.04%) and oxygen (<0.03%) at the end of the catalyst are predicted. For 4 SLPM the ethanol and oxygen conversion are predicted to be below 0.05% and 0.04%, respectively only for a C/O of 0.67 the conversion of ethanol is predicted to be 4.5%; for oxygen the conversion is predicted to be 2.0%.

It is expected that most of the fuel is converted in the first few millimeters of the catalytic section as was shown by many studies on CPOX of aliphatic hydrocarbons [21,25–27]. Consequently, there is little fuel left for homogeneous conversion in the current system, because it would take at least 8 mm after the hot zone of the catalyst (Fig. 13) until a sufficiently large radical pool is established to initiate significant homogeneous conversion, i.e. the ignition delay time is too large. A more quantitative analysis of the interaction of heterogeneous and homogeneous reactions in CPOX of ethanol over Rh will be presented in a forthcoming paper on modeling of the system under investigation.

5. Conclusions

The experimental results show that catalytic partial oxidation of ethanol on alumina-supported rhodium based catalyst is a promising opportunity to achieve high selectivity to hydrogen at short contact times. For low C/O, the selectivity to hydrogen is as high as predicted by computed equilibrium consideration, without by-product formation. The performed simulation of the homogeneous gas-phase reactions mechanism, as proposed by Marinov [28], leads to the conclusion that the gas-phase reactions play basically no role for fuel conversion under the experimental conditions presented in this work. Furthermore, the presented results allow the assumption that the alumina-support has a significant influence for the CPOX of ethanol on alumina-supported rhodium based catalysts, in case of high C/O and fuel-dilution. At C/O > 1.0 the product composition and fuel conversion are superimposed by deactivation of the catalyst due to coke formation. Regeneration of the catalyst is needed to establish equal starting conditions. The time to reach steady state depends on the C/O. In particular, at C/O of 1.20 and 4 SLPM it takes over 2900 s to reach steady state. At these conditions, also the yields vary qualitatively. In this paper the formation of significant amounts of diethyl ether in CPOX of ethanol at C/O > 1.20 is reported for the first time, to the best of our knowledge. Moreover, the results can now be used to support development of detailed surface reaction monarchisms.

Acknowledgements

Financial support by the Deutsche Forschungsgemeinschaft (DFG) is gratefully acknowledged.

N. H. thanks the Karlsruhe House of Young Scientists (KHYS) for the financial support of a research visit at the Norwegian University of Science and Technology (NTNU) and Anders Holmen and his group for the very good cooperation.

Appendix A. Supplementary data

Supplementary data associated with this article can be found, in the online version, at doi:10.1016/j.apcata.2010.08.055.

References

- [1] S. Cavallaro, *Energy & Fuels* 14 (2000) 1195–1199.
- [2] D.K. Liguras, D.I. Kondarides, X.E. Verykios, *Applied Catalysis B: Environmental* 43 (2003) 345–354.
- [3] S. Cavallaro, V. Chiodo, S. Freni, N. Mondello, F. Frusteri, *Applied Catalysis A: General* 249 (2003) 119–128.
- [4] E.C. Wanat, K. Venkataraman, L.D. Schmidt, *Applied Catalysis A: General* 276 (2004) 155–162.
- [5] N. Laosiripojana, S. Assabumrungrat, *Applied Catalysis B: Environmental* 66 (2006) 29–39.
- [6] A. Birot, F. Epron, C. Descorme, D. Duprez, *Applied Catalysis B: Environmental* 79 (2008) 17–25.
- [7] S. Liu, K. Zhang, L. Fang, Y. Li, *Energy & Fuels* 22 (2008) 1365–1370.
- [8] H.-S. Roh, Y. Wang, D.L. King, *Topics in Catalysis* 49 (2008) 32–37.
- [9] E.C. Wanat, B. Suman, L.D. Schmidt, *Journal of Catalysis* 235 (2005) 18–27.
- [10] J.R. Salge, G.A. Deluga, L.D. Schmidt, *Journal of Catalysis* 235 (2005) 69–78.
- [11] L.O.O. Costa, S.M.R. Vasconcelos, A.L. Pinto, A.M. Silva, L.V. Mattos, F.B. Noronha, L.E.P. Borges, *Journal of Materials Science* 43 (2008) 440–449.
- [12] A.M. Silva, A.M. Duarte de Farias, L.O.O. Costa, A.P.M.G. Barandas, L.V. Mattos, M.A. Fraga, F.B. Noronha, *Applied Catalysis A: General* 334 (2008) 179–186.
- [13] A.M. Silva, L.O.O. Costa, A.P.M.G. Barandas, L.E.P. Borges, L.V. Mattos, F.B. Noronha, *Catalysis Today* 133–135 (2008) 755–761.
- [14] S. Cavallaro, V. Chiodo, A. Vita, S. Freni, *Journal of Power Sources* 123 (2003) 10–16.
- [15] G.A. Deluga, J.R. Salge, L.D. Schmidt, X.E. Verykios, *Science* 303 (2004) 993–997.
- [16] L.D. Schmidt, R. Subramanian, J.R. Salge, G.A. Deluga, *Indian Chemical Engineer: Section B* 47 (2005) 100–105.
- [17] E. Vesselli, G. Comelli, R. Rosei, S. Freni, F. Frusteri, S. Cavallaro, *Applied Catalysis A: General* 281 (2005) 139–147.
- [18] H. Chen, H. Yu, Y. Tang, M. Pan, G. Yang, F. Peng, H. Wang, J. Yang, *Journal of Natural Gas Chemistry* 28 (2009) 191–198.
- [19] O. Akdim, W. Cai, V. Fierro, H. Provendier, A. van Veen, W. Shen, C. Mirodatos, *Topics in Catalysis* 51 (2008) 22–38.
- [20] M. Hartmann, S. Lichtenberg, N. Hebben, D. Zhang, O. Deutschmann, *Chemie Ingenieur Technik* 81 (2009) 909–919.
- [21] M. Hartmann, L. Maier, H.D. Minh, O. Deutschmann, *Combustion and Flame* 157 (2010) 1771–1782.
- [22] O. Deutschmann, S. Tischer, S. Kleditzsch, V.M. Janardhanan, C. Correa, D. Chatterjee, N. Mladenov, H. D. Minh, DETCHEM™ Software package, 2.2 ed., Karlsruhe, 2008. www.detchem.com.
- [23] A.L. Liberman, O.V. Bragin, T.V. Vasina, *Russian Chemical Bulletin* 13 (1964) 1266–1268.
- [24] H. Knözinger, *Angewandte Chemie International Edition* 7 (1968) 791–805.
- [25] R. Schwiedernoch, S. Tischer, C. Correa, O. Deutschmann, *Chemical Engineering Science* 58 (2003) 633–642.
- [26] R. Horn, K.A. Williams, N.J. Degenstein, A. Bitsch-Larsen, D. Dalle Nogare, S.A. Tupy, L.D. Schmidt, *Journal of Catalysis* 249 (2007) 380–393.
- [27] M. Hartmann, L. Maier, O. Deutschmann, *Applied Catalysis A: General*, doi:10.1016/j.apcata.2010.08.055.
- [28] N.M. Marinov, *International Journal of Chemical Kinetics* 31 (1999) 183–220.
- [29] D.O. Christensen, P.L. Silveston, E. Croiset, R.R. Hudgins, *Industrial & Engineering Chemistry Research* 43 (2004) 2636–2642.
- [30] S. Tischer, C. Correa, O. Deutschmann, *Catalysis Today* 69 (2001) 57–62.
- [31] L.L. Raja, R.J. Kee, O. Deutschmann, J. Warnatz, L.D. Schmidt, *Catalysis Today* 59 (2000) 47–60.